Check for updates

Original research article

SHM Structural Health Monitoring

Structural Health Monitoring
1–18
© The Author(s) 2026
Article reuse guidelines:
sagepub.com/journals-permissions
DOI: 10.1177/14759217261484120
journals.sagepub.com/home/shm
Sage

Guided wave-based SHM for testing – A composite fuselage under mechanical load

Maria Moix-Bonet[1], Benjamin Eckstein[2], Daniel Schmidt[1] and Peter Wierach[1]

Abstract

This study explores the use of guided wave-based structural health monitoring (GW-SHM) for structural testing of aircraft composite structures. The research presents the results of a full-scale test on a composite fuselage panel involving realistic impact damage, mechanical loading with three representative load cases, and temperatures ranging from 12 to 30°C. The dataset generated is then used to analyze the interaction between environmental and operational factors and damage effects on GW propagation. The analysis reveals that both load and temperature can cause variations in time-of-flight and amplitude of a similar order of magnitude, with temperature-induced changes distributed quite uniformly, while load effects exhibit a pronounced effect along the direction of the applied load. Furthermore, the detectability of realistic damage under varying environmental and operational conditions (EOCs) is examined. The full-scale structural test provides valuable insights into the implementation of GW-SHM in composite aircraft structures under varying load and temperature conditions. The results demonstrate that relevant impact damage can be detected under changing EOCs, confirming the suitability of the system for application in a full-scale fatigue test of a door surrounding structure.

Keywords

composite structures, environmental and operational conditions, structural testing, piezoelectric composites, piezoelectric transducer network

Introduction: Structural testing and SHM

Certification of composite aircraft structures and the damage tolerant design

The design of aircraft structures is driven by damage tolerance, a design philosophy developed in the 1970s. The damage tolerance approach requires structures to withstand pre-defined design loads in the presence of allowable damage until such damage can be detected by the maintenance strategy or other protocols in place.[1]

The use of composite materials in aircraft structures and the different behavior of metallic and composite materials lead to a redefinition of the relevant damage types and the mechanisms causing structural failure. One of the main differences affecting the methodology for fatigue and damage tolerance compliance is based on the damage growth mechanisms. Although composite structures can experience fatigue-induced damage, it can be addressed by suitable design and allowables. However, their impact sensitivity is a crucial factor in design and testing compared to fatigue behavior. Therefore, composite structures must be able to demonstrate residual strength at the end of the fatigue test and after being subjected to impact damage in order to be certified.[2]

The aviation certification agencies have issued new guidelines regarding the certification of aircraft composite structures using a damage-tolerant approach.[2,3] The guidelines define five damage categories, from low to high severity, and the loads that a structure with such damage must withstand. For example, category 1 damage is defined as barely visible impact damage (BVID) and allowed manufacturing defects. For

[1]German Aerospace Center e. V., Institute of Lightweight Systems, Braunschweig, Germany
[2]Airbus Operations GmbH, Bremen, Germany

Corresponding author:
Maria Moix-Bonet, German Aerospace Center e. V., Institute of Lightweight Systems, Lilienthalplatz 7, Braunschweig 38108, Germany.
Email: Maria.Moix-Bonet@dlr.de

category 1 damage, the structure is required to sustain a fatigue test corresponding to a full aircraft lifetime and afterwards still withstand ultimate load.

In aircraft design, structural tests are carried out to prove to certification authorities that a structure complies with the regulations. A test pyramid provides a systematic sequence of tests and analyses from coupon level through to full-scale structural validation. The validation of the fatigue and damage tolerance approach is ultimately performed by full-scale testing.[2] In a full-scale test, the specimen has the same dimensions as the original design and is considered to be fully representative.

SHM for a full-scale structure test

The validation tests of a damage tolerance design include the evaluation of representative damage inflicted on the structure. BVID and visible impact damage (VID) are introduced and then regularly inspected with non-destructive inspection (NDI) by certified inspectors throughout the validation test. This work considers the use of guided wave-based structural health monitoring (GW-SHM) for a full-scale structural test to monitor BVID and VID on a full-scale composite fuselage structure. The advantages of SHM for structural testing are, among others, test downtime reduction and a decrease in the monitoring interval.

Test downtime reduction. A full-scale fatigue test is an essential part of the development phase of an aircraft, and it is time-consuming. The full-scale fatigue tests required for the certification of the A320 lasted over several years and covered an equivalent of three times the aircraft's design lifetime.[4]

The overall duration of the development phase of a new aircraft and the subsequent ramp-up of production is of high relevance for an aircraft manufacturer company, as it impacts the return on investment of the development cost and the market success due to the reaction time to market needs. Accordingly, there is an incentive to shorten relevant tasks in the development phase such as the full-scale fatigue test. A considerable portion of the overall test time is test downtime, which is primarily determined by the scope of the NDI inspection program and the time needed to perform the required inspections at certain stops of the test, and to review and respond to the NDI results. Alternative solutions to current manual NDI include robotic and automated NDT techniques. However, these methods require sufficient space and a free, accessible surface to operate effectively. They can be cumbersome in confined or heavily instrumented areas, such as full-scale fatigue testing, and may interfere with existing cabling and imaging systems, such as DIC cameras. This highlights the interest in SHM as a suitable approach to structure monitoring.

One objective of the use of GW-SHM is therefore to spare a part of this test downtime by satisfying the need for an NDI inspection task instead by monitoring on demand or even continuously.

Continuous monitoring. The damage tolerance approach for composite structures classifies damage in three categories according to the growth rate: no-growth, slow growth, and arrested growth.[2] As the name indicates, no-growth damage does not increase in size, while slow growth damage increases slowly, stably, and predictably. In arrested growth, the damage is mechanically stopped before reaching a critical size, and it usually occurs due to design features, such as thickness variation or a structural joint.

For every structurally significant item, load cycling followed by a residual strength test is used to validate the sensitivity of the structure to damage growth. Assumptions on the growth rate of this damage are made to set the NDI intervals during fatigue testing. The inspection interval is defined so that assessments occur between the time the damage becomes detectable and the time the damage extent compromises the required residual strength,[2,5] much like it is done to determine the scheduled maintenance program. In a full-scale fatigue test, the inspection interval usually follows the in-service maintenance schedule, which considers the different damage categories, types, and growth behaviors.

With an automatized and permanently installed monitoring technology, such as GW-SHM, the time and effort dedicated to one inspection are greatly reduced, and a continuous monitoring is achievable. Continuous damage monitoring enables a better temporal allocation of damage changes and a faster reaction to unexpected damage growth behavior during fatigue testing.

The content of this work

This work investigates the suitability of GW-SHM for full-scale fatigue testing by examining an experimental test carried out on a full-scale composite door-surrounding structure under quasi-static flight-load conditions with the introduction of impact damage. Several reasons motivated the selection of these experimental tests to demonstrate the suitability of GW-SHM for this type of test. First, the representative fuselage section between the wing and the horizontal tail plane is the most complex part of the fuselage from a load-bearing standpoint, owing to the superposition

of different load components. It therefore provides a representative and certification-relevant environment for evaluating the damage detection capabilities of a GW SHM system. The potential application of GW-SHM for certification testing is not limited to this single structure; nevertheless, this particular configuration exemplifies the complexity of multi-axial loading and structural geometry. Second, in a certification test, compliance with the damage-tolerance approach must be demonstrated, for example, by introducing artificial damage and monitoring its growth to show that the structure meets the defined growth limits. Finally, by employing GW-SHM, the goal is to conduct measurements during an ongoing fatigue test to accelerate the certification process. This study therefore uses quasi-static load conditions as an initial, simplified step, allowing the suitability of GW-SHM to be assessed under challenging, yet operationally uncomplicated, conditions before progressing to dynamic fatigue loading.

This section establishes the framework and motivation for applying GW-SHM in full-scale fatigue testing within the aeronautical industry. The remainder of this work is organized as follows. The second section introduces the GW-SHM technique for damage identification in composite structures and reviews relevant literature regarding the influence of environmental and operational conditions (EOCs) in a SHM system. The third section provides a description of the composite fuselage structure, including details about the installed SHM system. The fourth section outlines the test campaign conducted on the structure, encompassing representative load cases for a fuselage structure. The extensive dataset, comprising GW measurements, as well as temperature and strain values, is analyzed in the fifth section. This publication concludes with summarizing remarks and acknowledgements.

Theoretical background: GWs under EOCs

Finding delamination and debonding in composite plate-like structures is one of the main potential applications of the GW-SHM technique in the aeronautical industry.[6,7] The sensitivity of GWs to this damage type, combined with the predisposition of composite laminates to accidental BVID, offers an interesting use case for GW-SHM. GW-SHM has been demonstrated as a monitoring technique to identify BVID in composite aircraft structures, typically in the form of delamination in the skin or debonding between skin and other structural elements.[8,9]

One of the main challenges for the application of this technique lies in the wide range of EOCs of an aircraft, as changes in EOC affect the propagation of GW. The GW-SHM technique typically relies on baseline-based methods for damage detection. This approach involves comparing data collected from the structure in its pristine state (the baseline) with data acquired at a later time. The baseline serves as a reference point, allowing the system to identify any anomalies that may indicate damage. Thus, a variation in the reference data set due to EOC deteriorates the system's ability to detect anomalies if not accounted for. Numerous techniques to compensate for EOC have been developed.[10–13] but an application in realistic conditions remains challenging for the available compensation techniques. Some of the challenges arise from the geometrical complexity of the monitored structure and the combination of multiple EOCs, such as load and temperature. Another key challenge is the amount of data required for some compensation techniques to operate effectively.

To significantly decrease the test downtime, the GW-SHM system should operate effectively within the temperature and load ranges commonly encountered in a structural test. Consequently, this study focuses on analyzing the variations a GW-SHM system experiences during representative EOC for a structural test.

Temperature

Among the operational and environmental variations encountered by an aircraft structure, temperature is one of the dominant effects on a GW-SHM system.[14] The effects of temperature on the GW propagation in composite materials have been extensively studied in the literature.[15,16] Temperature variations influence the response of a SHM system through multiple mechanisms.

The main influences reside in the thermal dependence of the piezoelectric effect, the material properties of the monitored structure, and the shear coupling between transducer and structure. Due to the integrated character of SHM transducer networks, these variations influence the response of a SHM system through multiple mechanisms.

On a material level, the stiffness of composite structures changes with temperature, affecting the group and phase velocities of GWs.[17] In addition to the arrival time, the stiffness variation influences the frequency domain through the wavelength tuning effect.[18,15] Since wavelengths are proportional to phase velocity, temperature influences the optimal frequencies for GW excitation.[19] Additionally, the thermal expansion and contraction of the material modifies the plate thickness as well as the distance between actuator and sensor.[10]

The bonding layer usually consists of a thin adhesive layer coupling the acoustic source and the

structure. Due to the finite thickness and stiffness of the bonding layer, the effective area of shear stress transmission is smaller than the transducer surface, an effect coined as shear lag.[20,21] The shear lag effect is dependent on the elastic constants of the bonding layer, transducer, and substrate, all regulated by temperature. As the shear lag effect increases with temperature, the effective area of the transducer decreases. As a consequence, the peak response of the GW-modes shifts toward higher frequencies. Moreover, a variation on the adhesive stiffness modifies the efficiency of the shear strain transmission. As the shear coupling between the transducer and the structure decreases, the efficiency of the energy transmission drops.[19]

Temperature affects the properties of piezoelectric ceramics as well. The piezoelectric coefficient d_{31} and the dielectric permittivity $e_{33}{}^{\sigma 15}$ increase with temperature and cause a counteracting effect on the voltage magnitude. The competing role of both parameters causes a maximal voltage response at an optimal temperature and a voltage response decrease with higher or lower temperatures.[19]

The effects of temperature on the propagation of GWs are numerous and have multiple origins. The dominant effect within the temperature range of interest is considered to be the change in elastic modulus of the monitored structure and bonding layer.

Loads

Structural loading causes deformation and stress, which in turn affect GW propagation. While a substantial body of research exists concerning the impact of temperature on GW behavior, fewer works have focused on understanding the behavior of GWs in stressed media, particularly in composite structures. The majority of the literature is based on the acoustoelastic effect, which describes the change in ultrasonic wave velocity in stressed solids.[22]

The acoustic-elastic effect of uniaxial tensile loading in isotropic metallic plates has been the subject of several studies. Chen et al.[23] showed that the acoustic-elastic effect is frequency-dependent, with the change in phase velocity increasing linearly with load at any given frequency. Furthermore, at a constant frequency, the transverse mode was found to be more sensitive to loading than the longitudinal mode. In the study by Gandhi et al.,[24] GW propagation in stressed solids exhibited anisotropic behavior in isotropic materials, with changes in phase velocity following a sinusoidal function along the direction of propagation. This anisotropic behavior led to a decrease in phase velocity in the direction of the tensile loading and an increase in phase velocity in the perpendicular direction. This trend was reproduced in the study by Pau et al.,[25] where a theoretical framework for nonlinear guided-wave propagation in prestressed plates showed the dependence between phase velocity and prestress state. Experimental studies by Roy et al.[26] demonstrated an increase in amplitude in the direction of tension, accompanied by a decrease in the transverse direction. The change in amplitude exhibited a linear relationship with load, similar to that observed in phase velocity.

Other works have explored the load effect in composite plates[27] and structures,[28] or in combination with temperature.[29] When comparing the stress effect in GFRP and aluminum plates under uniaxial tensile loading in the study by Palanisamy et al.,[27] the change in phase velocity was found to be one order of magnitude smaller on the GFRP specimen. Michaels et al.[29] quantified the combined effects of temperature and load variations on aluminum plates under uniaxial loading. Eckstein et al.[28] reported on the influence of loads on GW propagation in a composite fuselage. Using a network of piezoelectric transducers distributed throughout the structure, the complex loading conditions could be observed from the changes in group velocities. Recent works focused on simulating the effects of stress on GW propagating through both isotropic and anisotropic materials,[30] and on a Glass Fiber Reinforced Polymer (GFRP) spar under bending loads.[31]

The understanding of load effects on GW remains limited to specific cases, such as isotropic metallic materials and uniaxial loads. There is a lack of literature concerning load effects on piezoelectric transducers and the bonding layer between the host structure and transducers. This represents a significant gap in the current understanding of GW-SHM, particularly in more complex scenarios involving anisotropic materials, multiaxial stress, and transducer configurations.

Experimental setup

A GW-SHM system for a composite fuselage

A full-scale composite fuselage structure was designed and manufactured for the European-funded project MAAXIMUS with Airbus Operations, Airbus Helicopters, Premium Aerotec, Cotesa, and DLR as the main project partners involved.[32] The project aimed at developing highly integrated and precise design methods for aeronautical structures made of carbon fiber reinforced plastics (CFRP).[33] The design of the composite panel is representative for a passenger door region of a wide-body fuselage, such as the A350. The structure has dimensions of 4100 $\times$ 5700 mm and covers 9 frames, 17 stringers, 4 windows, and the door surround structure. An overview of the test structure is shown in Figure 1.

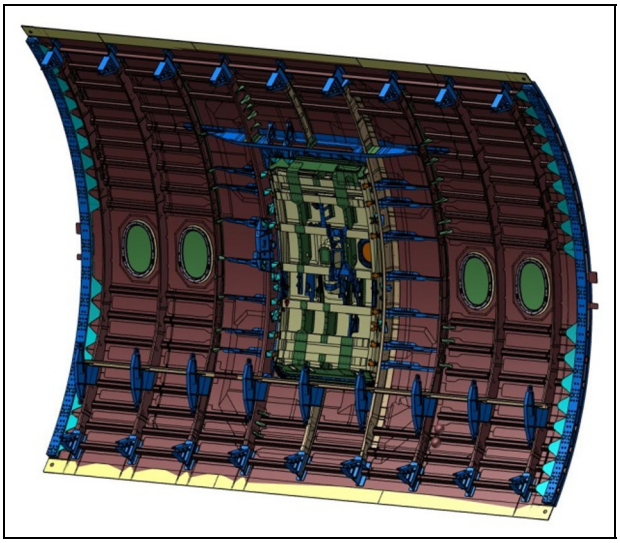


Figure 1. Full-scale demonstrator panel.[33]

A GW-SHM system was subsequently designed and installed on the fuselage panel. The design of the SHM system aimed for a practical application in an industrial environment. The distinguishing traits of this GW-SHM system are a robust transducer network, a reliable transducer connection, and a modular network concept.[34] The SHM system comprises three main components: a transducer network, a multiplexing-connecting unit, and a data acquisition platform.

The DuraAct™ transducer network. The transducer network was based on DuraAct™ piezocomposite transducers.[35] These transducers consist of a piezoceramic element embedded in a polymer matrix, providing improved robustness under mechanical loading and allowing installation on curved composite structures. Their suitability for quasi-static and fatigue loading conditions has been demonstrated in previous studies.[36,37]

A modular concept for a piezocomposite array was developed based on the DuraAct™ technology, displayed in Figure 2. Up to eight piezoelectric transducers are integrated into an array, including the wiring and a base plate to contact the piezoelectric transducers.

Multiplexing unit. The multiplexing module fulfills three main goals: a simple and reliable transducer connection, a significant cable reduction through multiplexing, and a cost and time-effective installation. The connector module's multiplexing function connects up to two transducers in parallel within the array for pitch-catch GW measurements. The modules are then attached to the data acquisition unit, connected in a daisy chain configuration. It is therefore possible to measure in pitch-catch configuration between any pair of transducers in the entire network with minimal cabling.

Data acquisition unit

The data acquisition is performed with a PXI system from National Instruments (Austin, Texas, USA), together with a software module for acquisition of GWs developed at DLR. The system combines an radio frequency (RF) switch matrix within the acquisition platform with the multiplexing functionality integrated into the piezocomposite arrays, enabling pitch–catch measurements across the entire network of 148 transducers while maintaining a limited cabling effort. The data were acquired with a sampling frequency of 10Ms/s and a 12-bit resolution, with excitation amplitudes up to 100 Vpp.

A fuselage panel under mechanical loading

To reduce the time and cost associated with full-scale fuselage barrel testing, a fuselage panel test aims to provide equivalent information at a lower level of the

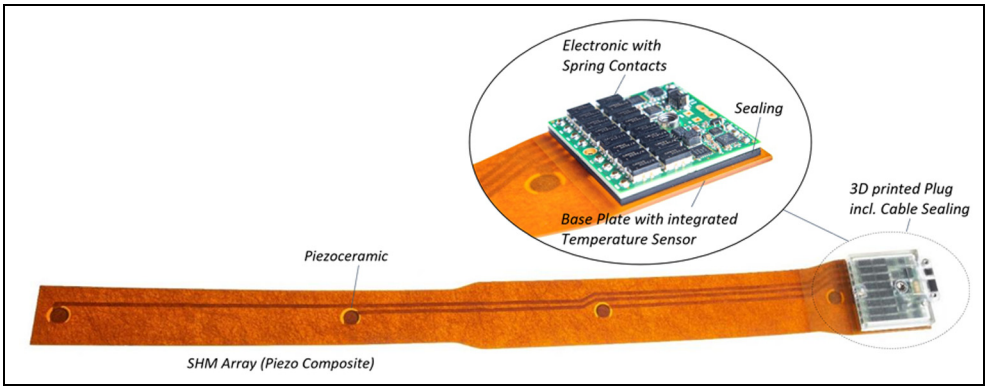


Figure 2. Piezocomposite array based on DuraAct™ with connector module.

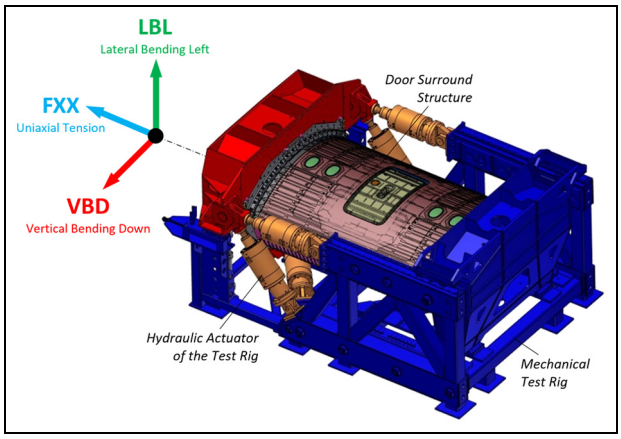


Figure 3. Test set-up: Door surround structure panel in test rig.[40]

test pyramid.[38] A large fuselage panel contains several critical structural features such as circumferential and longitudinal joints, the passenger door with the corresponding door surround structure, and representative floor structures.[39] A fuselage panel instrumented with a GW-SHM system was tested under representative loads using the test rig described in the study by Sachse et al.[40] and shown in Figure 3. The test rig consists of a fixed load frame and two bulkheads, one on each side. One bulkhead is fixed, while the other is movable for panel loading by means of a pneumatic system for pressure load application. This bulkhead has six hydraulic actuators, offering three degrees of freedom for displacement and three for rotation.

The loads in the panel are applied by the test rig through a set of hydraulic actuators. These loads reproduce conditions representative of those encountered by an aircraft in actual operation, such as lateral bending and vertical bending. Three load cases have been selected for the current study: uniaxial tension (FXX), lateral bending left (LBL), and vertical bending down (VBD). Figure 3 illustrates the basic load cases on a barrel level and the three selected load cases for the project. Although FXX is not a representative flight load, it was added for research purposes.

The three selected load cases were applied until a load equivalent to 75% of limit load (LL) in quasi-static test conditions. The LL is defined as the maximum load the aircraft should endure during normal operation. The quasi-static test stopped at several steps between the unloaded condition and 75% LL, allowing the SHM system to perform the measurements under static load conditions at multiple load levels.

Using a gas gun, impacts were applied according to the standardized method to create BVID.[2] The impactor contains a hemispherical projectile, measuring 25.4 mm in diameter and weighting 835 g, which is accelerated by means of compressed air. Impact damage was introduced in 11 locations, creating damage with sizes between 364 and 3720 mm^2. All impacts were classified as BVID and therefore as category 1 according to the European Union Aviation Safety Agency.[3] The gas gun introduced damage in the form of skin delaminations and debonding between the fuselage skin and adjacent structural elements, such as omega stringers, frames, and intercostals. The skin thickness at the impact locations ranged from approximately 2 to 7 mm.

NDI based on phased array ultrasonics was performed at the impact locations for reference purposes with an OmniScan MX from Olympus (Olympus Corporation, Tokyo, Japan). Figure 4(a) shows the C-scan of a delamination with an area of 580 mm^2, while the C-scan in Figure 4(b) reveals two small delaminated areas with sizes 9 × 8 and 10 × 10 mm. Their conjoint size is 26 × 14 mm, corresponding to a damaged area of 364 mm^2.

A test sequence was designed to assess the structure under various load cases and damage states, consisting of two load sequences: full and short. In the full load sequence, the structure experiences three load cases (FXX, LBL, and VBD) at eight defined load steps from

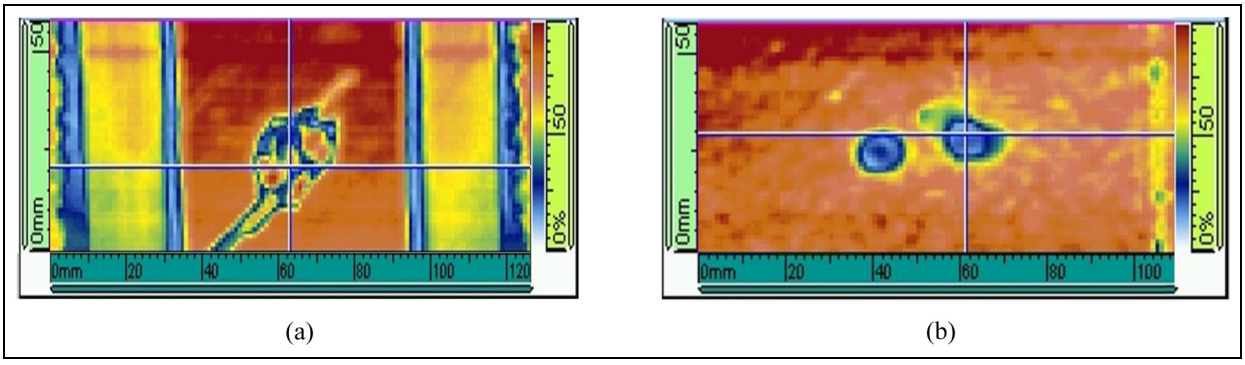


Figure 4. C-scan of ultrasound measurements after impacts (a) I12 with size 29 × 20 mm and (b) I03 with size 26 × 14 mm.

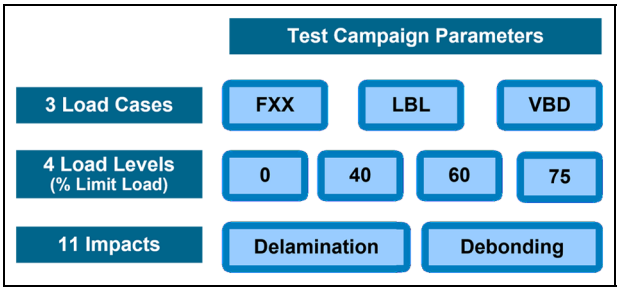


Figure 5. Parameters of fuselage panel test campaign.

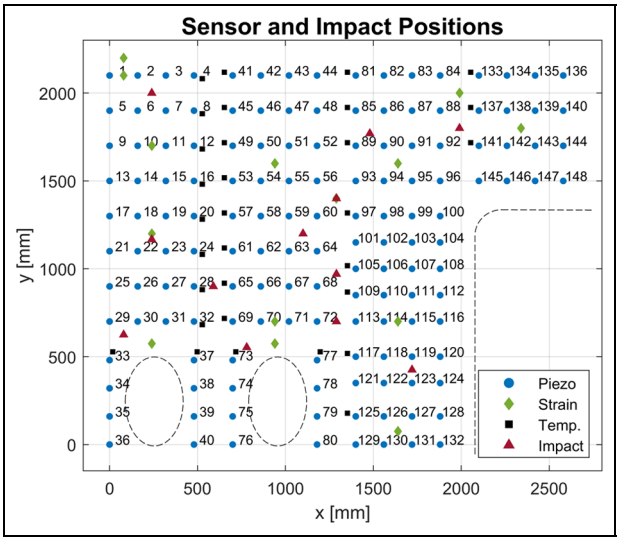


Figure 6. Sensor and impact positions on the top-left quadrant of the fuselage structure.

unloaded to 75% of LL. The short load sequence covers the same load cases but stops only at four defined load steps: unloaded, 20, 40, and 75% of LL.

The test campaign proceeded as follows: a full test sequence with the structure in a pristine (pre-damage) state, followed by short load sequences after each of the 11 impacts, concluding with a final full test sequence. The test parameters for the short load cycle are presented in Figure 5. This approach provides valuable data on the structure's behavior under various load conditions and damage states. The structure underwent a total of 12 load cycles, including three load configurations up to 75% of LL for each of the 11 damage states and an initial reference state.

The structure was instrumented with piezoelectric transducers, strain gauges, and temperature sensors. A total of 148 piezoelectric transducers, distributed in 31 piezocomposite arrays with integrated multiplexing function were installed on the top-left quadrant of the

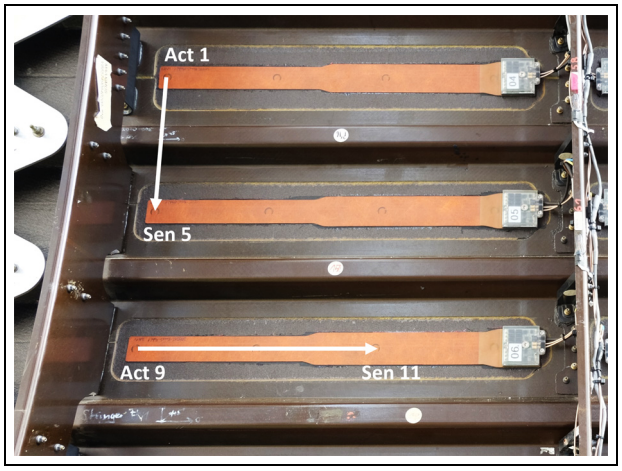


Figure 7. Section of fuselage structure with integrated transducer network and selected actuator–sensor paths.

fuselage structure. The piezoelectric transducers employed windowed five-cycle sinus burst excitation signals with frequencies between 50 and 200 kHz for GW actuation, capturing data from all actuator–sensor pairs within a 400 mm radius. Additionally, 31 temperature sensors and 14 strain gauges were distributed throughout the area covered by the piezoelectric transducers. The arrangement of sensor groups and impact positions on the top-left quadrant of the fuselage panel is presented in Figure 6, where the door and window cut-outs are depicted with dotted lines, providing a clear visualization of the test setup and key locations.

Results

This section explores two primary factors influencing GW propagation during a full-scale structure test: mechanical loading and temperature. The ability to identify damage using a GW-SHM system under these conditions is then discussed.

Load influence on GWs

To observe the influence of loads on GW propagation, a highly loaded and undamaged area with a strain gauge installed in the vicinity has been selected. Two actuator–sensor paths have been selected, one in the load direction and one at a 90° angle to the load direction. The first actuator–sensor path is used to observe the effects of tensile loading on GW propagation, while the second path provides transverse compression. The fuselage section under high loads is shown in Figure 7, with the selected actuator–sensor paths plotted on the illustration.

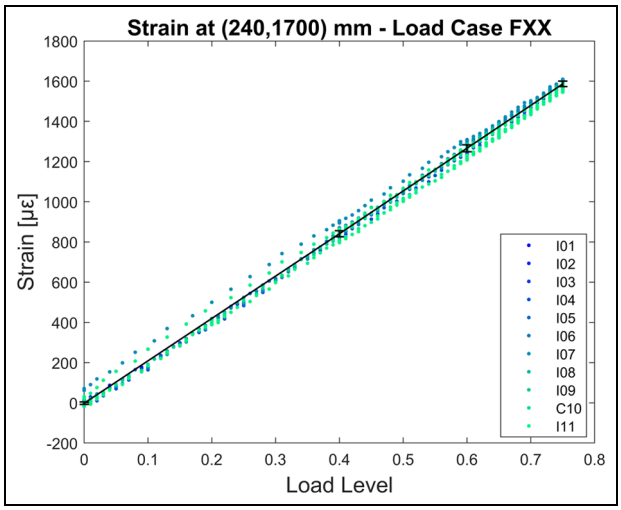


Figure 8. Strain values at position (240, 1700) mm in the longitudinal direction for load case FXX acquired between impact 1 (I01) and impact 11 (I11). Mean values and standard deviation in black. FXX: uniaxial tension.

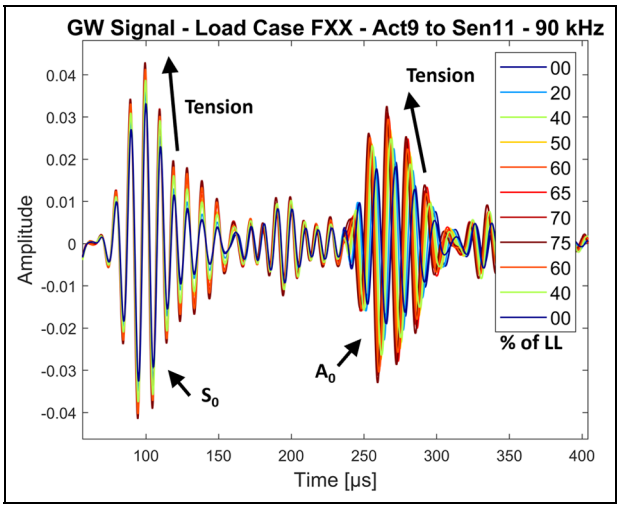


Figure 9. GW signal from actuator 9 to sensor 11 at 90 kHz – All load levels of FXX in reference state. GW: guided wave; FXX: uniaxial tension.

To monitor the strain on the area between transducers 9 and 11, the strain gauge installed at position (240, 1700) mm in the loading direction has been selected (see Figure 6). During the tensile load case (FXX), the strain in this direction reaches a maximum of 1587 με at 75 % of the LL, as shown in Figure 8. The strain values in Figure 8 are plotted as a function of the load level, defined as the percentage of the LL. Each load cycle across all damage states is represented in the figure, with colors distinguishing the damage states from 1st (I01) to 11th impact (I11). The mean strain values across all damage states and their corresponding standard deviation are indicated in black.

Strain readings change linearly with load, as expected for the linear elastic behavior of the structure. Thus, the next plots refer to the load level, knowing that the relationship between the local strain in the structure and the applied load level is linear.

To observe the effects of tensile loading on GW propagation, the signal response sent from actuator 9 and received by sensor 11 has been selected. The fuselage skin thickness in this area is approximately 2.1 mm, with two omega-stringer feet 53 mm from the transducers (see Figure 8).

The signal response for an actuation frequency of 90 kHz is plotted at several load levels in Figure 9. The two GW modes present at 90 kHz are highlighted in the plot: the symmetric (S_0) and anti-symmetric (A_0) fundamental modes. Both modes show increasing amplitude and decreasing time-of-flight (ToF) with tensile load.

The identification of GW modes is based on the expected group velocities and amplitudes of the fundamental modes at the selected actuation frequencies. In the present full-scale fuselage structure, ideal propagation conditions are not met due to spatial variations in lay-up and thickness, as well as the presence of structural elements such as stringers, frames, and clips. These features introduce scattering, reflections, and mode conversions, leading to the coexistence of multiple wave packets and limiting the extraction of pure A_0 and S_0 mode features. In this context, the measured signals are interpreted as being dominated by the fundamental modes, as typically defined in plate-like structures. These dominant arrivals are referred to as A_0 and S_0 modes, while acknowledging that mode mixing and wave interactions are inherently present in the considered configuration.

In order to quantify EOC effects, two features have been derived from the GW signal: amplitude and ToF. The amplitude is defined as the maximal amplitude of the Hilbert transform over the selected wave packet. The initial ToF computation is performed using cross-correlation between the actuation pulse and received signal, while changes in ToF due to load variations are determined through local temporal coherence of the cross-wavelet transform, as presented in the study by Eckstein et al.[41]

In Figure 10, the amplitude and ToF of the A_0-mode have been plotted as a function of the load level. The plots contain the selected features over a frequency range between 40 and 90 kHz. The trends observed at 90 kHz in Figure 9 are consistent across frequencies:

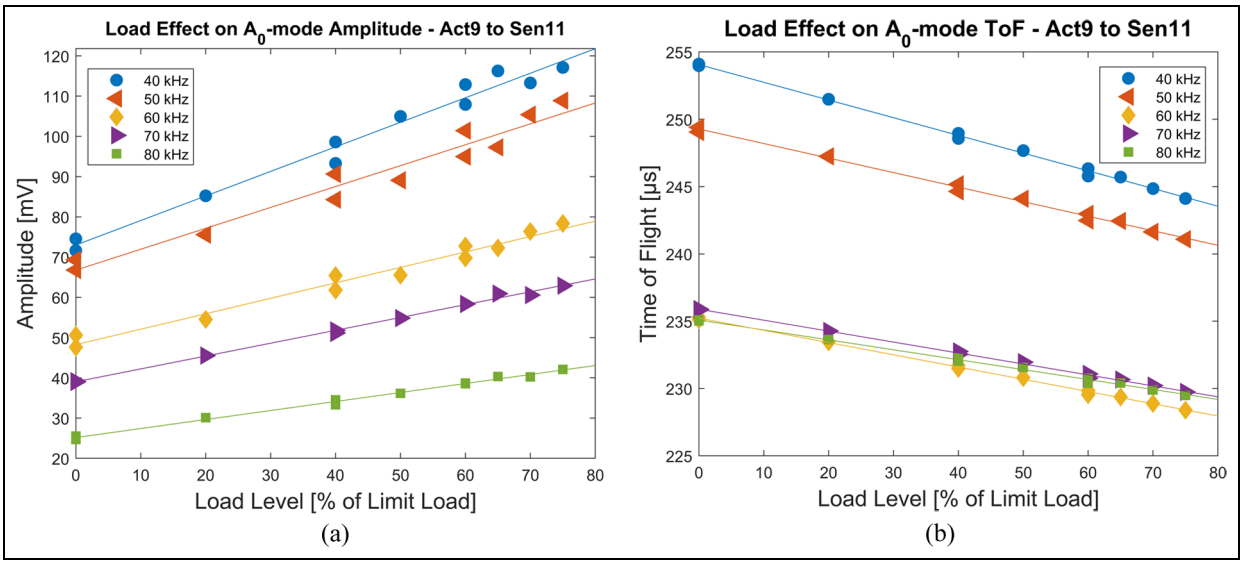


Figure 10. Effect of load case FXX on (a) amplitude and (b) ToF of A_0-mode from actuator 9 to sensor 11. FXX: uniaxial tension; ToF: time-of-flight.

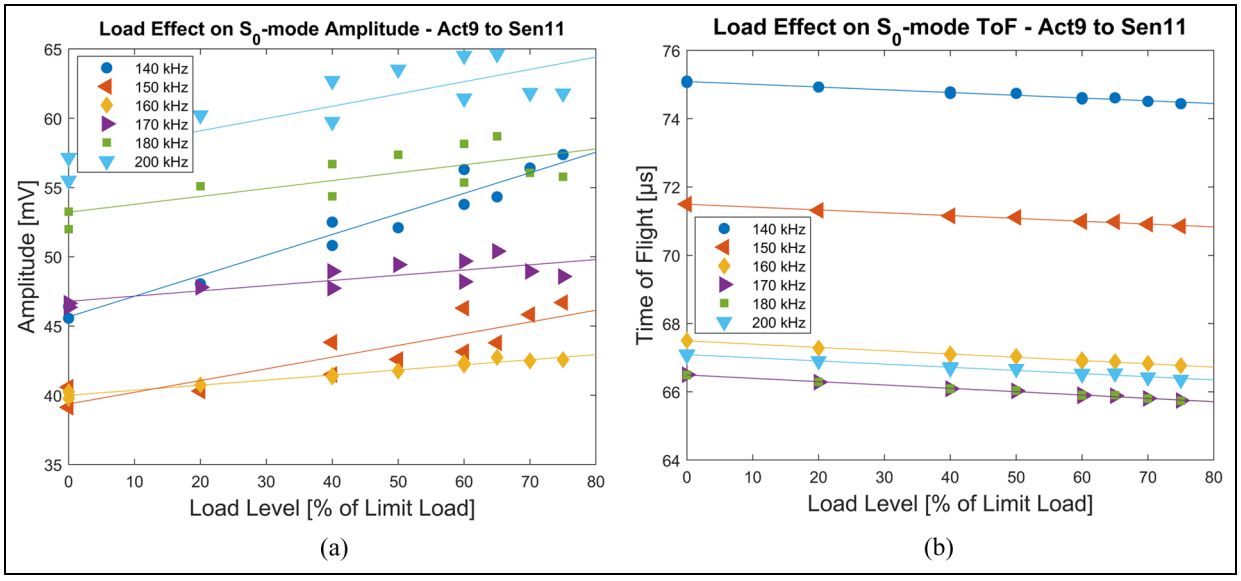


Figure 11. Effect of load case FXX on (a) amplitude and (b) ToF of S_0-mode from actuator 9 to sensor 11. FXX: uniaxial tension; ToF: time-of-flight.

amplitude rises and ToF falls with tensile stress. A linear regression has been fitted for each frequency, showing a good linear fit between the feature variation and the applied stress. In Figure 10, differences in amplitude values observed for identical load levels and frequencies are attributable to temperature variations, further discussed in "Temperature influence on GW" section.

In Figure 11, the amplitude and ToF have been plotted for the S_0-mode as well. A frequency range between 140 and 200 kHz has been chosen for the S_0-mode. Similarly, features vary linearly with load, though changes are smaller than for the A_0-mode. Amplitude values for S_0-mode show more scatter due to higher wave packet density, causing interference effects and complicating wave packet identification.

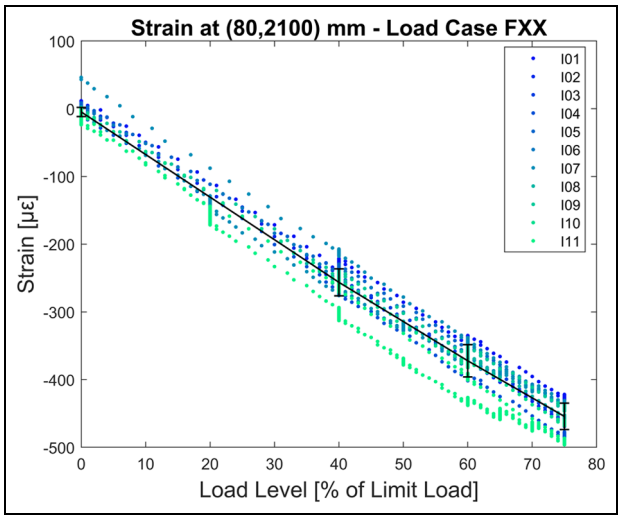


Figure 12. Strain values at position (80, 2100) mm in the transverse direction for load case FXX. Mean values and standard deviation in black. FXX: uniaxial tension.

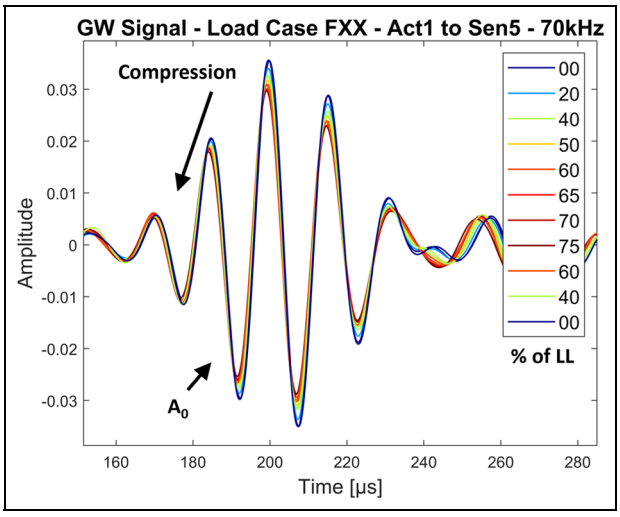


Figure 13. GW signal from actuator 1 to sensor 5 – All load levels of FXX in pristine state. GW: guided wave; FXX: uniaxial tension.

Having chosen the path from actuator 1 to sensor 5 to observe the effect of transverse compression, the strain gauge closest to the area was selected. Installed at (80, 2100) mm perpendicular to the tensile load (see Figure 6), the strain gauge measured -454 με at 75% of LL. Analogous to the tension case, the strain values have been plotted in Figure 12. Compared to the tension example, the strain magnitude is lower, and the standard deviation is slightly higher than in tension.

The GW signal at 70 kHz for the A_0-mode of transducer pair 1–5 is plotted for several load levels in Figure 13. Compressive stress reduces both amplitude and ToF. In compression, the same effect as tension is observed for the ToF, while the opposite effect is found for the amplitude.

In Figure 14, amplitude and ToF of the A_0-mode have been plotted as a function of the load level for frequencies between 40 and 90 kHz. Compressive stresses induce an amplitude drop of approximately 19.7% and a minimal ToF decrease, less than 1 μs. The linear relationship between signal features and load is observed in the compression case as well.

The study reveals increased guided-wave sensitivity to stress at lower frequencies. At a fixed frequency, the A_0 mode exhibits higher sensitivity to load variations than the S_0 mode, consistent with literature reporting that the fundamental flexural mode is most responsive to mechanical loading.[23]

For a given frequency, a near-linear relationship is observed between applied load and variations in both ToF and amplitude. This behavior is consistent with previous studies,[23,24] which report linear changes in phase velocity under constant frequency conditions. Although ToF variations are inversely related to phase velocity changes, a linear velocity variation is reflected as an approximately linear ToF variation at the considered scale. Furthermore, the observed load sensitivity decreases with increasing frequency, while preserving this linear trend, in agreement with Gandhi et al.[24]

In contrast to classical acoustoelastic results for isotropic metallic plates, the present data show a decrease in ToF for both tensile and compressive loading. In isotropic systems under uniform uniaxial stress, tensile and compressive states typically produce opposite trends in guided-wave velocity depending on propagation direction.[25] The sign of the acoustoelastic response in such systems is governed by the interaction of material and geometric nonlinearities and is strongly influenced by the third-order elastic constants.

The effect of guided-wave propagation in anisotropic composite structures has not been as extensively studied, and direct comparison with isotropic metallic plate behavior is not straightforward. In addition, such models assume homogeneous and often uniaxial stress states. In the present fuselage structure, these assumptions are not fulfilled. Due to the presence of geometric discontinuities such as the door cutout and stiffening elements (e.g., omega stringers), the applied loads are redistributed, resulting in a multiaxial and spatially varying stress field. The skin primarily carries in-plane membrane stresses (σx, σy, τxy), with local stress concentrations and shear components, particularly near structural discontinuities. As a consequence, GW propagation along the actuator–sensor paths occurs under non-uniform and multiaxial stress conditions rather than pure tension or compression.

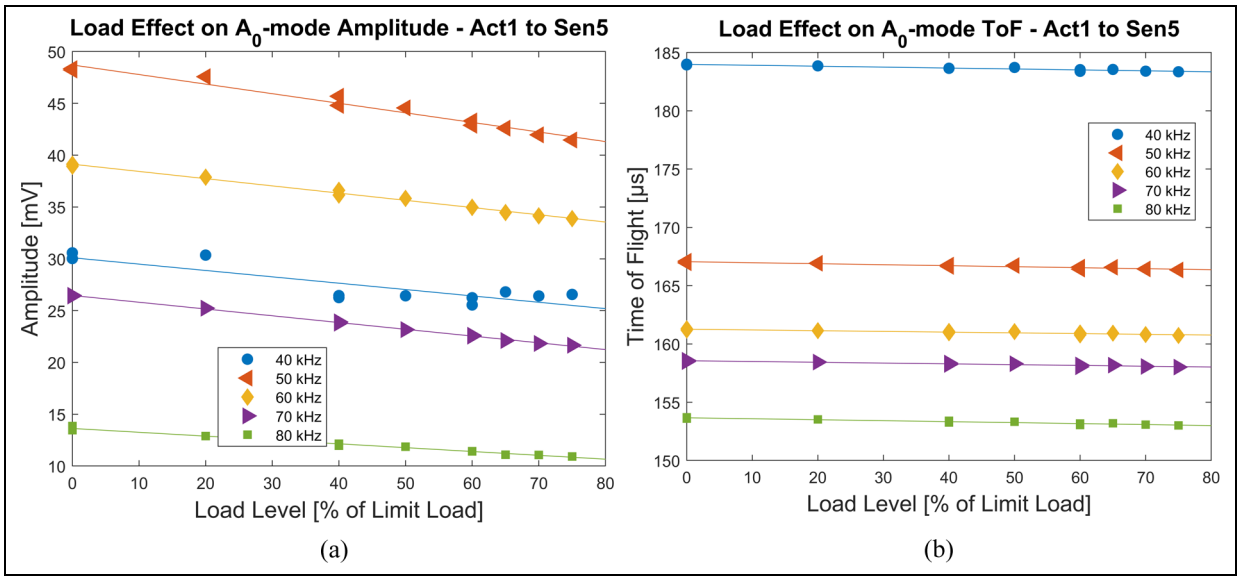


Figure 14. Effect of load case FXX on (a) amplitude and (b) ToF of A_0-mode from actuator 1 to sensor 5. FXX: uniaxial tension; ToF: time-of-flight.

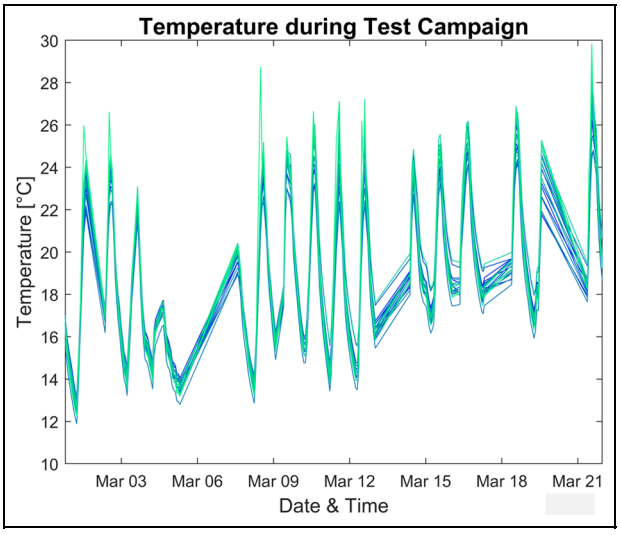


Figure 15. Temperature of fuselage structure during test campaign.

This multiaxial stress state, combined with structural anisotropy, mode conversions, and wave packet interactions, limits direct comparison with isotropic plate behavior reported in the literature. The observed ToF reduction under both tensile and compressive loading should therefore be interpreted as the result of combined material, geometric, and structural wave propagation effects rather than classical isotropic acoustoelastic behavior.

Temperature influence on GW

The test campaign was carried out over a period of 3 weeks in a non-climate-controlled hangar, resulting in GW measurements acquired between 12 and 30°C. Temperature sensors distributed throughout the monitored area recorded the temperature at the start of each GW measurement. The temperature measurements displayed in Figure 15 show the daily temperature fluctuations as well as an increasing average temperature as the test progressed.

In Figure 16, the amplitude and ToF of the A_0-mode at 70 kHz for the 9-to-11 path are plotted as a function of load level over 12 load cycles (corresponding to the 12 damage states). Each data point is color-coded according to the temperature during acquisition. The dominant trend in Figure 16 is consistent with "Load influence on GWs" section: amplitude increases and ToF decreases with increasing load. A 60.6% amplitude increase and a 6.2 µs ToF decrease are attributed to mechanical loading. A superimposed variability of approximately 10% in amplitude and 2.5 µs in ToF is not explained by load and is attributed to temperature effects.

Analogously, Figure 17 shows the response for the 1-to-5 path under compression. Here, amplitude decreases by 19.7%, and ToF decreases by less than 1 µs due to load. As in the tensile case, additional variability of approximately 10% in amplitude and approximately 2 µs in ToF is observed, attributed to temperature changes.

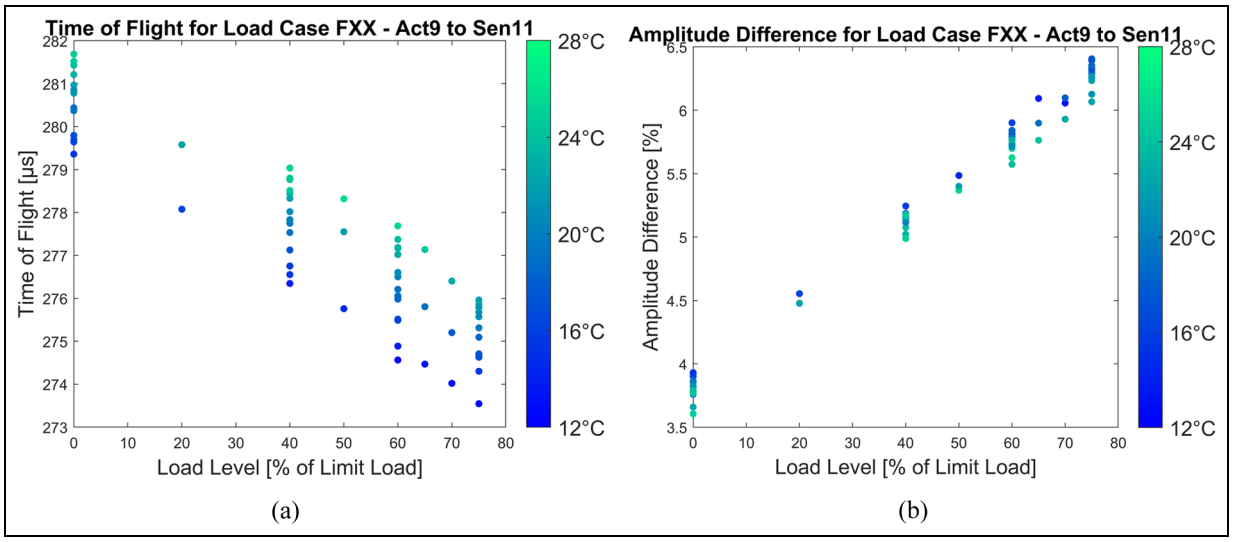


Figure 16. (a) ToF and (b) amplitude versus load level for A_0-mode between actuator 9 and sensor 11 at 70 kHz. ToF: time-of-flight.

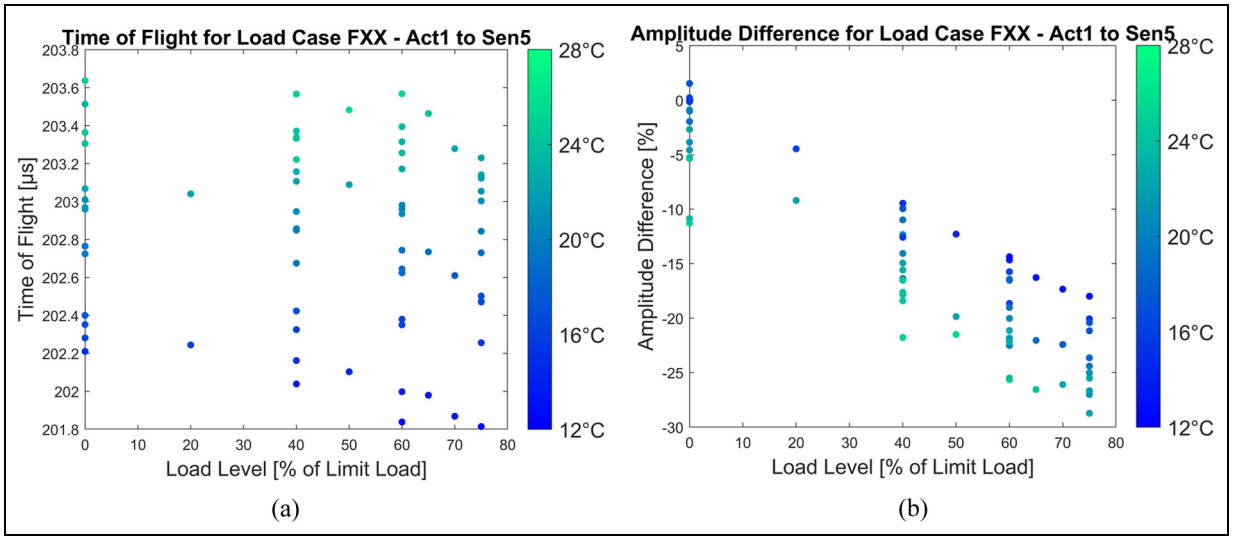


Figure 17. (a) ToF and (b) amplitude versus load level for A_0-mode between actuator 1 and sensor 5 at 70 kHz. ToF: time-of-flight.

In both compressive and tensile loading scenarios, the impact of temperature is consistent: a temperature rise results in ToF increase and amplitude reduction. These observations are in agreement with existing literature[17,42]: The decrease in stiffness of the composite material due to temperature results in higher ToF and lower amplitude values.

To facilitate a comparison between the effects of mechanical load and temperature, Table 1 presents normalized sensitivity measures in terms of ToF and amplitude variations per unit strain and per temperature change. The normalized sensitivities show that temperature and mechanical loading have effects of the same order of magnitude on guided-wave propagation. Consequently, both influences should be considered when interpreting GW measurements in realistic environments.

The values are derived from the two exemplary actuator–sensor paths (1–5 and 9–11) and correspond to different experimental cases, which differ in terms of loading direction and structural setup. Therefore, the reported sensitivities are intended to provide an order-of-magnitude comparison of the environmental and operational effects and are not directly comparable or generalizable to the entire fuselage structure.

Table 1. Effects of temperature and mechanical load on GW propagation.

Load effects on A_0-mode (70 kHz)	Tension	Compression	Temperature
ToF	−3.9 μs ToF/1000 με	−1.3 μs/1000 με	1.2 μs/10°C
Amplitude	38.2%/1000 με	−43.4%/1000 με	−11%/10°C

GW: guided wave; ToF: time-of-flight.

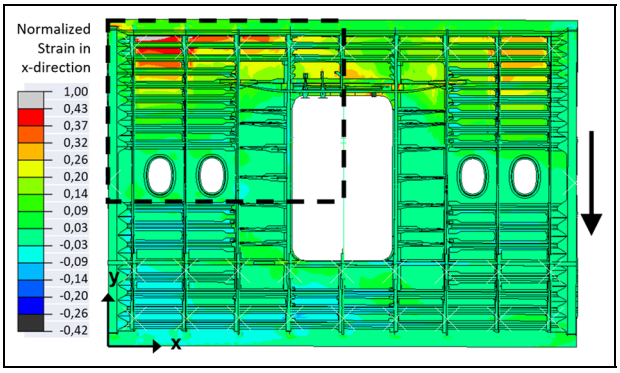


Figure 18. Normalized strain in flight direction for VBD load case. VBD: vertical bending down.

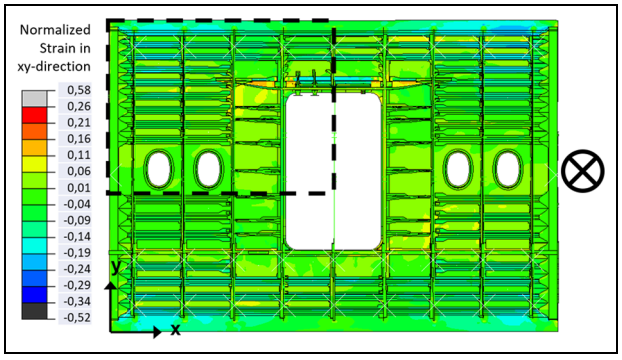


Figure 19. Strain at 45° of flight direction for LBL load case. LBL: lateral bending left.

Changes in GW propagation on large structures

While "Load influence on GWs" and "Temperature influence on GW" sections focused on the effects observed for a single path, the complexity of the current application scenario lies in the extensive SHM sensor network, with hundreds of actuator–sensor paths being monitored. GW propagation varies across paths due to local load and temperature conditions, structural geometry, and material properties. An effective damage identification must account for these variations across the network.

To illustrate the variation between load cases, the simulated strain has been plotted for two representative load cases. The simulation model was developed within the MAAXIMUS project[31] and customized to fit the boundary conditions of the present structural test. The load introduction in this study has been simplified compared to real fuselage loading, resulting in different strain distributions.

Figure 18 shows the normalized strain in the longitudinal axis (flight direction) for the VBD load case. The left side of the panel was fixed on the test rig, while the load was applied via hydraulic cylinders attached to the right side (see Figure 3). The quadrant of the structure monitored with the SHM system is highlighted, where high positive strain values are observed in the left-top corner.

In Figure 19, the normalized strain is illustrated for the LBL load case, for the direction at a 45° angle to the longitudinal and normal axes. The load is applied in the direction of the transverse axis, bending the fuselage inward. The area on the top-left of the door cut-out exhibits the highest positive strain values, while the top-left corner of the structure presents negative strain values.

As in section 4.1, the strain causes changes in the ToF and amplitude of GW modes. The changes on ToF between the unloaded state and the two load cases, VBD and LBL, at 75% of LL have been calculated for all actuator–sensor paths with a maximal length of 300 mm. The analysis is based on signals acquired at an actuation frequency of 70 kHz. For this frequency, the ToF of the dominant wave packet, corresponding to the A_0 mode, was extracted and compared for each actuator–sensor path. As discussed previously, pure mode propagation cannot be assumed in the present fuselage structure, and local wave packet interferences may influence the measured ToF values. Nevertheless, the resulting ToF variations provide a consistent indication of the strain-induced trends across the sensor network.

In Figure 20, the shift in ToF is shown, with actuator–sensor paths colored according to the observed change in ToF.

The areas of the fuselage with the highest shift in ToF are roughly in agreement with the high positive strain zones indicated in Figures 18 and 19. When the structure is subjected to the VDB load case, the larger time shift values for GWs are in the longitudinal

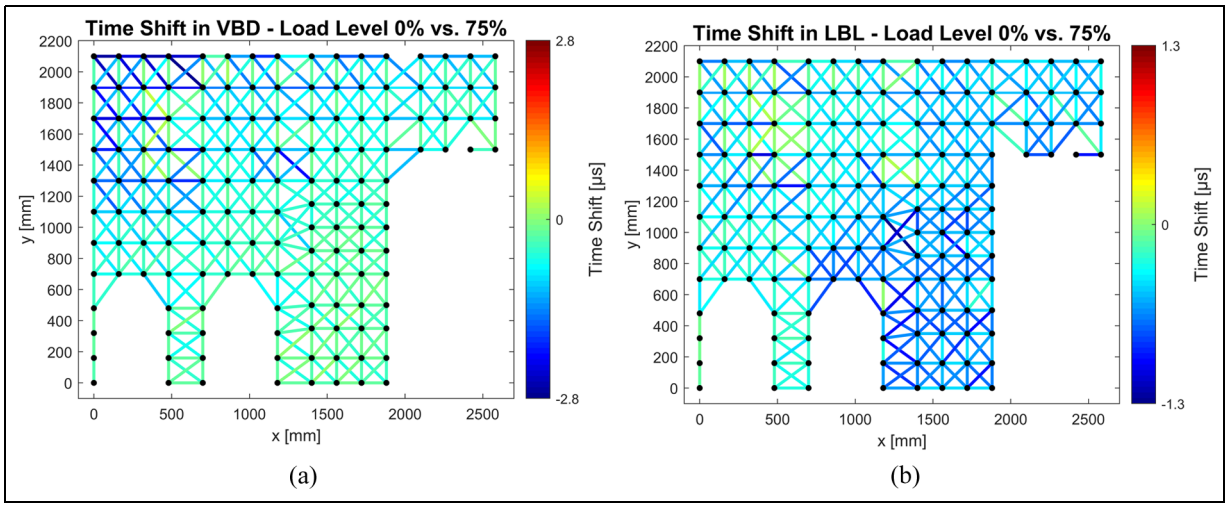


Figure 20. Difference in ToF for load cases VBD and LBL at 75% of LL: (a) time shift in VBD – load level 0 versus 75% and (b) time shift in LBL – load level 0 versus 75%. ToF: time-of-flight; VBD: vertical bending down; LBL: lateral bending left; LL: limit load.

direction at the top-left corner. The higher values in time shift to the left of the door cut-out during the LBL load case match the area of highest positive strain values in Figure 19. Figure 20 shows that both positive and negative strain lead to an increase in wave velocity.

During the 3-week test campaign, structure temperature varied between 12 and 30°C, affecting GW measurements across the monitored area. The temperature-induced effects across the approximately 5 m^2 of monitored surface are visually represented in Figure 21. The central region presents larger signal changes, indicating stronger temperature variations.

Temperature and load exhibit a comparable effect on GW propagation. Changes in load and temperature result in variations in ToF and amplitude of a similar magnitude. However, the distribution of these changes across a complex structure diverges. Temperature-induced variations tend to be evenly distributed and consistent in all directions. In contrast, the distribution of load-induced changes exhibits a pronounced effect along the direction of the applied load.

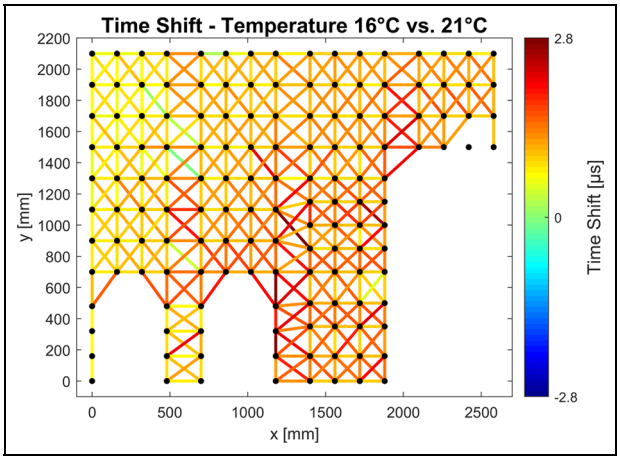


Figure 21. Difference in ToF for a 5°C temperature difference in unloaded state. ToF: time-of-flight.

Damage detection under changing EOC

This section assesses the damage detection capability of the GW-SHM system for BVID detection in a composite fuselage structure under combined load and temperature variations representative of a non-climatized hangar.

To examine the influence of damage combined with load and temperature, two actuator–sensor paths featuring damage presence have been selected. In Figure 22, amplitude and ToF are graphically presented twice: (a) highlighting the dominant EOC factor and (b) differentiating between two damage states.

The damage case in Figure 22(a) corresponds to a path in a highly loaded region affected by a delamination introduced during the test campaign, measuring 29 × 20 mm in size (see Figure 4(a)). Load-induced variations dominate ToF and amplitude, but a consistent amplitude reduction is observed across all load levels, indicating damage presence.

In contrast, the second actuator–sensor path is situated in a lightly loaded area with temperature variations between 12 and 28°C. Here, temperature is the dominant EOC. Two smaller delaminations with a joint area of 26 × 14 mm (see Figure 4(b)) have been introduced. While the selected features separate

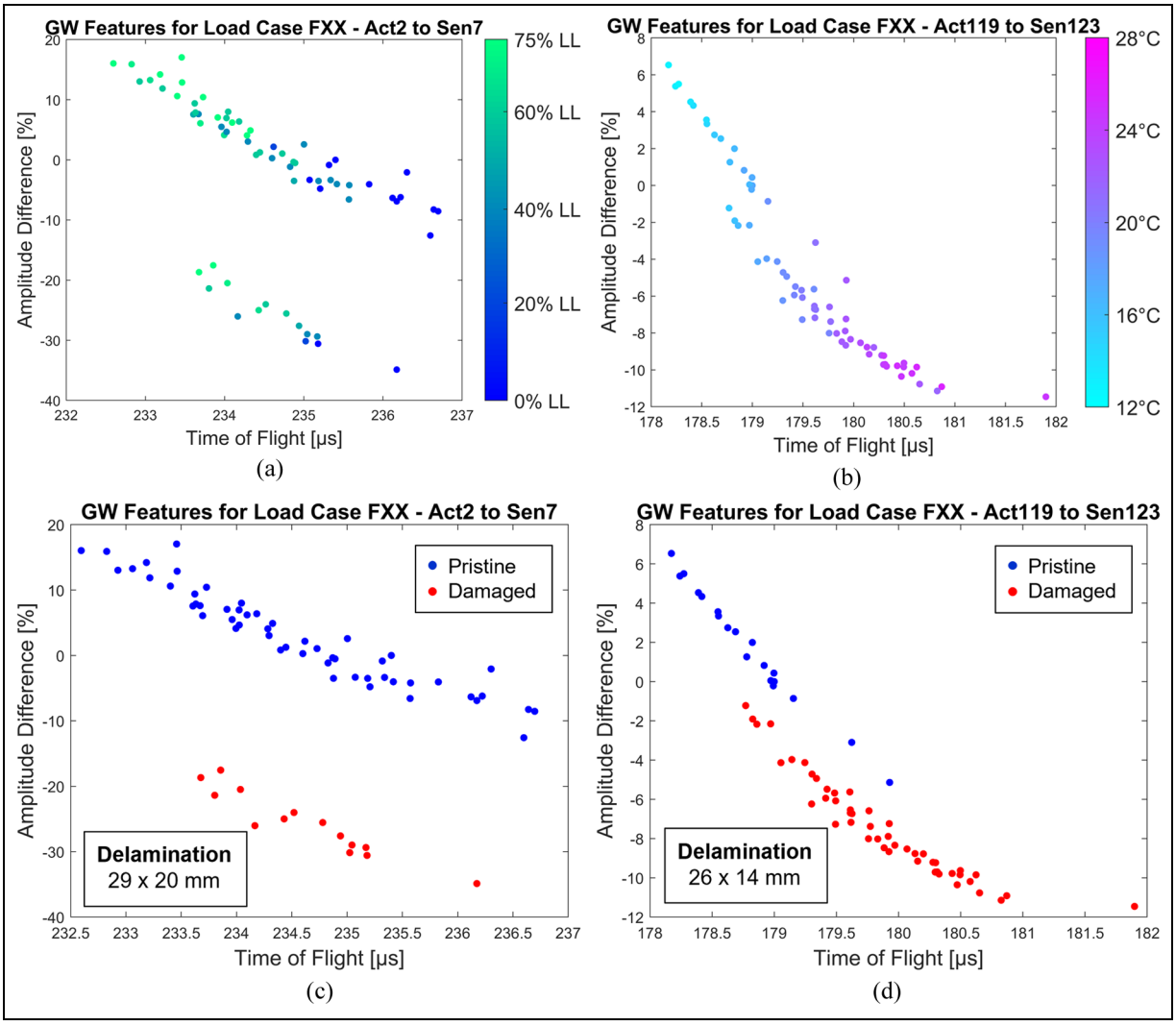


Figure 22. Amplitude difference and ToF of A_0-mode at 70 kHz of two paths with damage presence, highlighting the dominant EOC (a) and (b) and the damage state (c) and (d). ToF: time-of-flight; EOC: environmental and operational condition.

damage effects from thermal effects, the subtlety of the damage effects requires a more precise damage detection strategy.

Overall, the results in Figure 22 indicate that the GW-SHM system can detect relevant damage during full-scale fatigue testing of a fuselage structure. Clear separation between damaged and undamaged states is achieved across all 11 damaged areas under varying EOC. While larger damage (Figure 22(c)) may be identified without accounting for load and temperature effects, the detection of smaller damage (Figure 22(d)) requires explicit consideration of load and temperature in a data-driven framework.

A key challenge is the high variability of GW responses combined with limited training data for data-driven methods. This variability originates from complex and changing EOC conditions as well as structural heterogeneity in a full-scale fuselage, where no two actuator–sensor paths are identical. One possible way forward is the use of uncertainty-aware learning methods such as Gaussian Processes. A preliminary investigation using Gaussian Processes on this dataset is presented in the study by Moix-Bonet et al.[43]

In the context of full-scale fatigue testing, the GW-SHM system requires an initial training phase during test commissioning and early fatigue loading. This need for training data aligns with the sequence of certification fatigue tests. Typically, three times the aircraft design service goal are simulated by three test phases. Damage is not expected at the beginning of the first phase, while phases two and three require demonstration of damage tolerance. As inspection effort increases

over time, SHM can provide a significant monitoring advantage without being compromised by the initial training requirement.

Concluding remarks

A GW-SHM system has been successfully deployed and tested on a full-scale composite fuselage structure under representative mechanical loading, impact damage, and environmental variations. The resulting dataset captures the combined influence of load, temperature, and damage on guided-wave propagation in a realistic fuselage structure.

The results show that GWs are more sensitive to mechanical loading at lower frequencies, with the A_0 mode exhibiting higher sensitivity than the S_0 mode. For both loading directions, a near-linear relationship is observed between load and variations in ToF and amplitude. In contrast to classical acoustoelastic behavior in isotropic metallic plates, the measured ToF decreases under both tensile and compressive loading. This deviation may be related to the combined effects of CFRP anisotropy, differing material properties compared to metallic systems, multiaxial stress states, structural discontinuities, and wave–structure interactions.

Temperature and mechanical loading induce guided-wave variations of similar order of magnitude, but with fundamentally different spatial characteristics: temperature effects are broadly distributed, while load effects are strongly direction-dependent.

A qualitative analysis was conducted to determine the feasibility of discriminating between EOC-induced changes and variations in signals caused by damage. Damage detection remains feasible under varying EOCs; however, performance depends on damage size and location. While certain damage could be detected without additional EOC information, instances with smaller damage sizes or complex geometries required the integration of EOC data along with multiple signal features to effectively distinguish between pristine and damaged states. A key challenge remains the high signal variability under changing conditions combined with limited training data.

Overall, the study demonstrates the feasibility of GW-SHM for full-scale composite structures under certification-relevant conditions and highlights both the potential and limitations of current interpretation approaches in complex anisotropic structures.

Ultimately, the authors view the full-scale structural test as a door opener for the usage of GW-SHM in aircraft composite structures with a damage-tolerant design. A successful implementation of the GW-SHM technique for structural testing can accelerate its development and increase the acceptance and visibility of GW-SHM as an alternative to conventional NDI for composite aeronautical structures.

Acknowledgements

Without the allocation of the necessary funds, the implementation of the project would not have been possible. This research project has been funded by the Federal Ministry of Economics and Climate Protection (BMWK) within the framework concepts of LuFo V and LuFo VI with grant agreement numbers 20Q1725D and 20D2105G. The project results achieved are the result of close cooperation between the partners involved. The piezocomposite arrays were manufactured and installed by Invent GmbH, the mechanical tests and the NDI were performed by Applus+ IMA, while the fuselage panel was generously made available by Airbus Operations GmbH.

ORCID iDs

Maria Moix-Bonet https://orcid.org/0000-0002-1327-0080
Benjamin Eckstein https://orcid.org/0009-0003-6073-2756
Daniel Schmidt https://orcid.org/0009-0004-5722-2891
Peter Wierach https://orcid.org/0000-0003-0852-9112

Ethical considerations

Ethical approval was not required for this study, as it did not involve human participants, human data, or human tissue.

Consent to participate

Not applicable, as this study did not involve human participants.

Consent for publication

Not applicable, as this study did not involve individual person data or images.

Funding

The authors disclosed receipt of the following financial support for the research, authorship, and/or publication of this article: This research project has been funded by the Federal Ministry of Economics and Climate Protection (BMWK) within the framework concepts LuFo V and LuFo VI with grant agreement numbers 20Q1725D and 20D2105G.

Declaration of conflicting interests

The dataset generated and analyzed during the current study is not publicly available due to commercial restrictions and proprietary confidentiality agreements.

Data availability statement

The dataset generated and analyzed during the current study is not publicly available due to commercial restrictions and proprietary confidentiality agreements.

References

1. European Union Aviation Safety Agency. EASA, *Easy access rules for large aeroplanes (CS-25)* (initial issue). EASA, 2018, pp. 197–201.
2. Federal Aviation Administration. *Certification and compliance considerations for aircraft products with composite materials*. (FAA), U.S. Department of Transportation, 2018.
3. European Union Aviation Safety Agency. AMC 20-29 composite aircraft structure. *Annex II to ED Decision 2010/003/R*. Cologne, European Union Aviation Safety Agency, Germany, 2010, pp. 1–36.
4. Hilfer G, Rößler N, Peters C, et al. A320 ESG full scale fatigue test – lessons learned. In: Komorowski J (ed.) *ICAF 2011 structural integrity: influence of efficiency and green imperatives*. Springer, 2011, pp. 529–537. https://doi.org/10.1007/978-94-007-1664-3_42
5. Heida JH and Grooteman FP. *Airframe inspection reliability using field inspection data*. National Aerospace Laboratory NLR/Report number: NLR-TP-98144, 1998.
6. Rose JL. Successes and challenges in ultrasonic guided waves for NDT and SHM. In: *Proceedings of the national seminar & exhibition on non-destructive evaluation*, Indian Society for Non-Destructive Testing (ISNT), Tiruchirappalli, India, 10–12 December 2009.
7. Gorgin R, Luo Y and Wu Z. Environmental and operational conditions effects on Lamb wave based structural health monitoring systems: a review. *Ultrasonics* 2020; 105: 106114. https://doi.org/10.1016/J.ULTRAS.2020.106114
8. Ricci F, Monaco E, Maio L, et al. Guided waves in a stiffened composite laminate with a delamination. *Struct Health Monit* 2016; 15(3): 351–358. https://doi.org/10.1177/1475921716636335
9. Moix-Bonet M, Eckstein B, Loendersloot R, et al. Identification of barely visible impact damages on a stiffened composite panel with a probability-based approach. In: *10th International workshop on structural health monitoring*, DEStech Publications, Inc., Stanford, CA, USA, 1–3 September 2015.
10. Konstantinidis G, Drinkwater BW and Wilcox PD. The temperature stability of guided wave structural health monitoring systems. *Smart Mater Struct* 2006; 15(4): 967. https://doi.org/10.1088/0964-1726/15/4/010
11. Farrar CR and Worden K. *Structural health monitoring: a machine learning perspective*. Wiley, 2012.
12. Abbassi A, Römgens N, Tritschel FF, et al. Evaluation of machine learning techniques for structural health monitoring using ultrasonic guided waves under varying temperature conditions. *Struct Health Monit* 2022; 22(2): 1308–1325. https://doi.org/10.1177/14759217221107566
13. Giannakeas IN, Sharif Khodaei Z and Aliabadi MH. An up scaling temperature compensation framework for guided wave–based structural health monitoring in large composite structures. *Struct Health Monit* 2023; 22(2): 777–798. https://doi.org/10.1177/14759217221095415
14. Wang D, Ye L, Lu Y, et al. Probability of the presence of damage estimated from an active sensor network in a composite panel of multiple stiffeners. *Compos Sci Technol* 2009; 69(13): 2054–2063. https://doi.org/10.1016/j.compscitech.2008.11.005
15. Lanza di Scalea F and Salamone S. Temperature effects in ultrasonic Lamb wave structural health monitoring systems. *J Acoust Soc Am* 2008; 124(1): 161–174. https://doi.org/10.1121/1.2932071
16. Lu Y and Michaels JE. Feature extraction and sensor fusion for ultrasonic structural health monitoring under changing environmental conditions. *IEEE Sens J* 2009; 9(11): 1462–1471. https://doi.org/10.1109/JSEN.2009.2019339
17. Raghavan A and Cesnik CES. Effects of elevated temperature on guided-wave structural health monitoring. *J Intell Mater Syst Struct* 2008; 19(12): 1383–1398; https://doi.org/10.1177/1045389X07086691
18. Giurgiutiu V. Tuned Lamb wave excitation and detection with piezoelectric wafer active sensors for structural health monitoring. *J Intell Mater Syst Struct* 2005; 16(4): 291–305. https://doi.org/10.1177/1045389X05050106
19. Matt HM. *Structural diagnostics of CFRP composite aircraft components by ultrasonic guided waves and built-in piezoelectric transducers*. PhD dissertation. University of California, San Diego, CA, 2007.
20. Sirohi J and Chopra I. Fundamental understanding of piezoelectric strain sensors. *J Intell Mater Syst Struct* 2000; 11(4): 246–257. https://doi.org/10.1106/8BFB-GC8P-XQ47-YCQ0
21. Giurgiutiu V. *Structural health monitoring with piezoelectric wafer active sensors*. Academic Press, 2008.
22. Hughes DS and Kelly JL. Second-order elastic deformation of solids. *Phys Rev* 1953; 92(5): 1145. https://doi.org/10.1103/PhysRev.92.1145
23. Chen F and Wilcox PD. The effect of load on guided wave propagation. *Ultrasonics* 2007; 47(1–4): 111–122; https://doi.org/10.1016/J.ULTRAS.2007.08.003
24. Gandhi N, Michaels JE and Lee SJ. Acoustoelastic Lamb wave propagation in biaxially stressed plates. *J Acoust Soc Am* 2012; 132(3): 1284–1293. https://doi.org/10.1121/1.4740491
25. Pau A and Lanza di Scalea F. Nonlinear guided wave propagation in prestressed plates. *J Acoust Soc Am* 2015; 137(3): 1529–1540. https://doi.org/10.1121/1.4908237
26. Roy S, Lonkar K, Janapati V, et al. A novel physics-based temperature compensation model for structural health monitoring using ultrasonic guided waves. *Struct Health Monit* 2014; 13(3): 321–342. https://doi.org/10.1177/1475921714522846
27. Palanisamy R, Haq M, Deng Y, et al. *Structural health monitoring: influence of stress fields in propagation of guided waves in composite*, https://speautomotive.com/wp-content/uploads/2021/02/ET_Palanisamy_Structural-Health-Monitoring-Influence-of-Stress-Fields-in-Propagation-of-Guided-Waves-in-Composites.pdf (2021, accessed 30 September 2026).
28. Eckstein B, Bach M and Moix-Bonet M. Analysis of loading effects on guided ultrasonic waves and damage assessment in a full-scale CFRP fuselage structure. *Struct Health Monit* 2015; 5: 19–25. https://doi.org/10.12783/SHM2015/5

29. Michaels JE, Michaels TE, Lee SJ, et al. *Understanding and exploiting the effects of loading on ultrasonic sensing systems for structural health monitoring*. Air Force Research Laboratory (AFRL)/Report number: AFRL-RX-WP-TR-2012-0280, 2012.
30. Dalmora A, Imperiale A, Imperiale S, et al. A time-domain spectral finite element method for acoustoelasticity: modeling the effect of mechanical loading on guided wave propagation. *Wave Motion* 2024; 129: 103328. https://doi.org/10.1016/j.wavemoti.2024.103328
31. Perfetto D, Lamanna G, Petrone G, et al. A modelling technique to investigate the effects of quasi-static loads on guided-wave based structural health monitoring systems. *Forces Mech* 2022; 9: 100125. https://doi.org/10.1016/j.finmec.2022.100125
32. EU-funded Project MAAXIMUS, https://cordis.europa.eu/project/id/213371
33. Kruse F, Kühn M, Krombholz C, et al. Production of a full scale demonstrator-structure within the FP7 project "Maaximus". In: *5th International workshops on aerostructures*, EASN Association, UK, 2–4 September 2015.
34. Schmidt D, Moix-Bonet M, Galiana S, et al. *Integration von angepassten und dezentralen Structural Health Monitoring Systemen in Faserverbundstrukturen*. Deutscher Luft-Und Raumfahrtkongress (DLRK), 2023.
35. Wierach P, Monner HP, Schoenecker A, et al. Application-specific design of adaptive structures with piezoceramic patch actuators. In: *International society for optics and photonics*, SPIE, San Diego, CA, USA, 2002.
36. Salmanpour MS, Sharif Khodaei Z and Aliabadi MH. Airborne transducer integrity under operational environment for structural health monitoring. *Sensors* 2016; 16: 2110. https://doi.org/10.3390/s16122110
37. Moix-Bonet M, Buethe I, Bach M, et al. Durability of co-bonded piezoelectric transducers. *Procedia Technol* 2014; 15: 638–647. https://doi.org/https://doi.org/10.1016/j.protcy.2014.09.025
38. Bakuckas JG, Bigelow CA, Tan PW, et al. Full-scale testing of fuselage panels. In: *2001 IEEE autotestcon proceedings. IEEE systems readiness technology conference*, IEEE, Valley Forge, PA, USA, 20–23 August 2001, pp. 827–846.
39. Goldbach S, Franke R and Dresden I. Materials and NDT applications in aircraft component development tests. In: *DGZfP-Proceedings BB 124-CD, DGZfP (German Society for Non-Destructive Testing)*, Vol. 124, 2010.
40. Sachse M, Götze M, Nebel S, et al. Testing approach for over wing doors using curved fuselage panel testing technology. In: Niepokólczycki A and Komorowski J (eds) Lecture Notes in Mechanical Engineering (LNME), Springer Nature Switzerland AG, 2020, pp. 831–837. https://doi.org/10.1007/978-3-030-21503-3_65
41. Eckstein B, Moix-Bonet M and Bach M. Analysis of environmental and operational condition effects on guided ultrasonic waves in stiffened CFRP structures. In: *7th European workshop on structural health monitoring*, NDT.net, Nantes, France, 8–11 July 2014, pp. 495–502.
42. Moll J, Kexel C, Pötzsch S, et al. Temperature affected guided wave propagation in a composite plate complementing the Open Guided Waves Platform. *Sci Data* 2019; 6(1): 1–9. https://doi.org/10.1038/s41597-019-0208-1
43. Moix-Bonet M, Schmidt D, Eckstein B, et al. Damage detection in composite aircraft fuselages under load and temperature using Gaussian processes for GW-SHM. In: *15th European workshop on structural health monitoring*, DEStech Publications, Inc., Stanford, CA, USA, 9–11 September, 2025.